IV.I.6 Networks of Boron-Doped Carbon Nanopores for Low-Pressure Reversible Hydrogen Storage

Peter Pfeifer[1,2] (PI), M. Frederick Hawthorne[1,2,3] (Co-PI), and Carlos Wexler[1,2] (Co-PI)
[1]Department of Physics and Astronomy, University of Missouri
[2]Alliance for Collaborative Research in Alternative Fuel Technology, University of Missouri
[3]International Institute of Nano and Molecular Medicine, University of Missouri
Peter Pfeifer, Phone: (573) 882-2335, E-mail: pfeiferp@missouri.edu

Contract Number: DE-FG02-07ER46411

Date: April 24, 2009
Project Period: August 15, 2007 – August 14, 2010
Reporting Period: August 15, 2008 – April 24, 2009

Program Scope

This project is an integrated synthesis/characterization/computational effort to develop novel materials – monolithic boron-doped carbon made from polymeric precursors, crisscrossed by networks of nanopores – expected to have superior hydrogen storage capacities not available in other materials. The aim is to develop a fundamental understanding of the mechanisms by which boron, through its electron-deficient electronic structure and long-range effect on distant carbon atoms, combined with appropriate pore geometries, creates deep potential wells which can hold films of physisorbed molecular hydrogen at densities much higher than undoped carbon. Such high-density films and their understanding at the molecular, statistical mechanical, and macroscopic thermodynamic level are critical for the rational design of high-performance materials with controlled reversible storage characteristics at low pressure and room temperature. The project supports one of the high-priority research directions of the National Hydrogen Storage Project.

I. Recent Experimental Accomplishments

High Capacity Materials: Biocarbon, and Polymer-Based; Undoped and Doped with Boron

Various nanoporous carbons were analyzed for their potential to store hydrogen. Table I describes some of the systems analyzed, including two generations of undoped activated biocarbon (from corncob), two boron doped activated biocarbons, and three carbons based on synthetic polymers.

Figure 1 presents adsorption isotherms (80 K) for some of these samples. It is worth noting the significant increase in storage capacity of the new generation of activated carbons, 3K and 4K, vs. the older Batch 5.1. Sample 4K shows very high cryogenic storage capacity (14 wt% at 90 bar). Increasing the KOH-to-carbon ratio increases storage capacity (sample 4K vs. 3K), even though the surface area remains essentially the same. This suggests an increase of the fraction of high binding energy sites from 3K to 4K, by a mechanism yet to be understood. Early generations of polymer-based activated carbons (S7, S8, P11) show promise as hydrogen storage media, considering that some of them already show excess adsorption comparable to some of our best biocarbons. To normalize samples with different surface areas and pore volumes, we analyze H_2 uptake in terms of *areal excess adsorption* (gravimetric

TABLE I. High-Capacity Nanoporous Carbons

Sample	Description	Activation & Doping	BET Σ (m^2/g)	H_2 excess ads. (g/kg @ 50 bar, 80 K)
3K	Biocarbon (corncob)	KOH:C = 3:1 (wt)	2,500	63
4K	Biocarbon (corncob)	KOH:C = 4:1 (wt)	2,600	73
Batch 5.1	Biocarbon (corncob)	KOH:C = 2:1 (wt)	3,100	44
3K-H7	Biocarbon, $B_{10}H_{14}$ (liquid)	KOH:C = 3:1 (wt)	1,500	52
3K-H6	Biocarbon, $B_{10}H_{14}$ (vapor)	KOH:C = 3:1 (wt)	2,400	68
S7	Pyrolysis of Saran (polyvinylidine chloride)	400°C (HCl release)	625	24
S8;0K-4B ^ b	Pyrolysis of Saran + $K_2B_{12}H_{12}$	$K_2B_{12}H_{12}$, 790°C	N/A	34
P11;3K-5B ^ e	Pyrolysis of copolymer (polymethylene polyphenylisocyanate/Castor oil/H_3BO_3/epoxy oil) & KOH activation	Pyrolysis at 480°C; activation, with KOH:C = 3:1 (wt) at 790°C	N/A	60

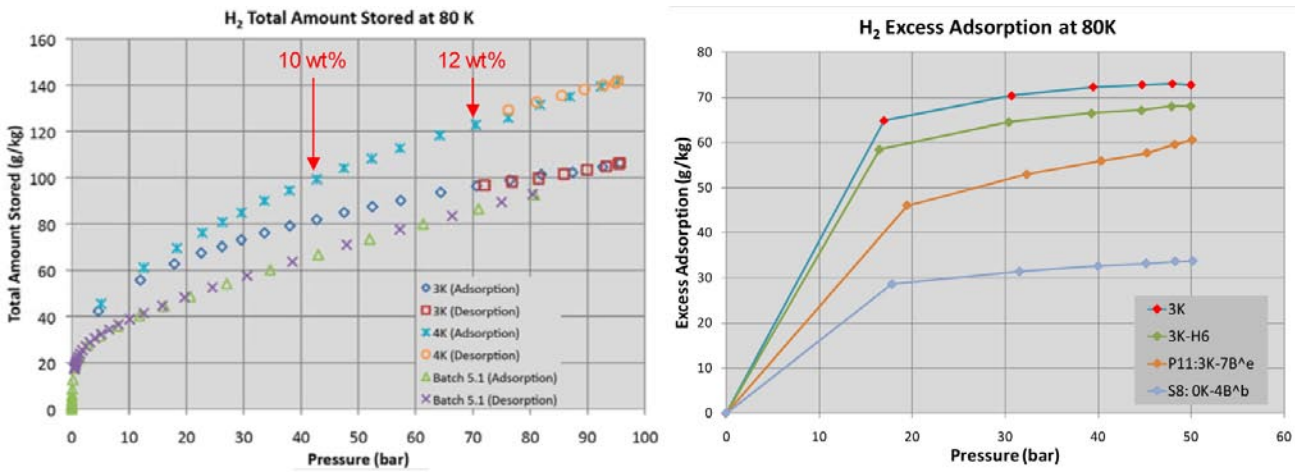

FIGURE 1. Hydrogen adsorption isotherms for various carbon materials. Left: Total amount stored on boron-free biocarbons (precursors for B-doping with decaborane) activated with 3:1 and 4:1 ratios of KOH:C. Sample 4K reaches ~14 wt% at 90 bar and 80 K. Right: gravimetric excess adsorption for corn cob and polymeric precursors.

excess adsorption divided by BET surface area), which depends only on how strongly the surface adsorbs H_2 (but not on pore volume and surface area of the sample), and is a direct, (p, T)-dependent measure of the H_2 binding energy. Table II lists results for B-doped biocarbons. For B-free carbons, the highest areal excess adsorption at 50 bar and 80 K, 38 µg/m^2, is found for the polymer-based Sample S7, which is 36% higher than the best biocarbon value, 28 µg/m^2, for Sample 4K (see Table I). This is remarkable because it suggests that pore spaces can be engineered, toward high binding energies of H_2 on pure carbon, even more successfully than previously known (see Figure 2 and Ref. 1).

Boron Doping I: Liquid vs. Vapor Phase Deposition

Decaborane ($B_{10}H_{14}$) was identified as the most suitable compound for boron deposition onto high-surface-area, boron-free carbons. Decaborane is a stable crystalline solid, melts at 100°C, boils at 213°C (1 bar), and easily sublimes under moderate vacuum. With a molecular diameter of ~5 Å, it can easily reach all pores of interest in our biocarbon samples. At 200-250°C, it decomposes into nonvolatile hydrides, $B_{10x}Hz$, and H_2. Boron deposition occurs by the reaction

$$x\mathrm{B_{10}H_{14}} + \mathrm{C}_y \xrightarrow{200\text{-}250^\circ\mathrm{C}} \mathrm{B}_{10x}\mathrm{H}_z(\mathrm{ads}) + \mathrm{C}_y + (7x - z/2)\mathrm{H_2}$$

$$\mathrm{B}_{10x}\mathrm{H}_z(\mathrm{ads}) + \mathrm{C}_y \xrightarrow{500\text{-}600^\circ\mathrm{C}} \mathrm{B}_{10x}\mathrm{C}_y + z/2\ \mathrm{H_2}$$

Three methods of carrying out the reaction were developed. In Method I (liquid deposition), $B_{10}H_{14}$ is deposited as a thin liquid film, followed by thermal decomposition of $B_{10}H_{14}/B_{10x}H_z$. In Method II (liquid-vapor deposition), a submonolayer of $B_{10x}H_z$ is created by thermal decomposition of $B_{10}H_{14}$ liquid/vapor (admixed $B_{10}H_{14}$), followed by thermal decomposition of $B_{10x}H_z$. In Method III (vapor deposition), a submonolayer of $B_{10x}H_z$ is created by decomposition of $B_{10}H_{14}$ vapor (sublimation of $B_{10}H_{14}$ in a separate chamber), followed by thermal decomposition of $B_{10x}H_z$.

Prompt gamma neutron activation analysis (PGNAA, $^{10}B + n \rightarrow {}^{7}Li + {}^{4}He + \gamma$) at the University of Missouri Research Reactor is used to characterize the boron content of the doped materials, and areal excess adsorption was used to analyze the benefits of the different methods. Table II summarizes our results, including gravimetric and areal excess adsorption. Method I (liquid deposition) appears most efficient in delivering B, but reduces surface area, presumably by

TABLE II. Analysis of Samples Doped by Decaborane Decomposition

Sample (Method)	B:C (mix)	B:C (PGNAA)	BET Σ (m^2/g)	H_2 gravim. excess ads. (g/kg @ 50 bar, 80 K)	H2 areal excess ads. (µg/m^2 @ 50 bar, 80 K)
3K (precursor)	0	0	2,500	63	25
3K-H7 (I)	0.088	0.060	1,500	52	34
3K-H6 (II)	0.018	0.014	2,400	68	28
3K-H5 (III)	N/A	0.008	2,800	62	22

partial blocking of pores with B. Method II (liquid/vapor deposition) does not appear to block pores significantly and delivers a sizeable amount of B. Method III (vapor deposition) needs to be cycled to achieve significant doping. For a doping level of 6 wt%, a significant positive net effect of B-doping is observed: 3K-H7 has ~50% higher areal excess adsorption than 3K.

Boron Doping II: Copolymerization

The use of nanoporous biocarbon for B-doping – vs. fabrication of B-doped nanoporous carbon from boron-containing synthetic polymers – has been convenient because of the preexisting large surface areas in biocarbons. The results for doping with decaborane, in which the presence of boron in the activated carbons has been validated experimentally and the predicted increase in storage capacity per unit area with increasing boron content has been demonstrated, make a strong case that introduction of boron through synthetic polymers – copolymerization of carbon-carrying monomers and boron-carrying monomers – will generate materials with enhanced storage capacities. We have already fabricated several polymer-based carbons doped with boron by a variety of methods, with excess adsorption competitive with that of our best biocarbons (see Table I). Of particular interest is the unexpected result that Saran-based carbon, without boron, exhibits the highest areal excess adsorption observed in our laboratory (Sample S7 in Table I). Structural work on S7, to better understand this result, is presented in Figure 3. For the polymers with boron, work is in progress investigating how boron can be incorporated in the feedstock so that boron *substitutionally* displaces carbon in the final nanostructure (rather than forming patches or adatoms of boron), how different concentrations of boron (stoichiometric vs. non-stoichiometric) affect the electronic structure of the doped material and the associated functional implications for adsorption of H_2.

Hydrogen Binding Energy: Models for Adsorption

The nanoporous carbon storage capacities found so far have lead us to understand that a pore-space architecture that simultaneously maximizes gravimetric and volumetric storage capacities will likely consist of graphitic sheets that hold 2-3 layers of H_2 between adjacent sheets. Pore-size distributions from N_2 BET indicate the presence of pore sizes from sub-nm to several nm in width. Analysis of H_2 adsorption isotherms for various samples show that a two-binding-energy (BE) model for adsorption (narrow pores = large BE, wide pores = small BE) is adequate. (Figure 2; see also Section II.)

Characterization of Pores: Subcritical Adsorption of N_2 and Small-Angle X-Ray Scattering (SAXS)

Nitrogen adsorption isotherms from 10^{-7} to 1 bar at 77 K were measured for many carbons. Additional characterization was performed using SAXS. Figure 3 shows a N_2 adsorption analysis and SAXS analysis of the Saran-based carbon S7 (not doped, not activated with KOH, pores created by effluent HCl during pyrolysis) $-[(CH_2)-(CCl_2)]- \rightarrow 2C + 2HCl$). The presence of mesopores is evident, but the bulk of the pore volume resides in micropores. The bimodal pore-size distribution is also seen in the SAXS spectrum.

II. Recent Theoretical and Computational Accomplishments

Quantum Rotors, Adsorption and a New Characterization Technique for Sub-nm Pores

Most simulations treat the molecules of H_2 as a point-like object (orientation unspecified), or at best consider a classical rigid-rotor model (2 angles). However, since hydrogen is so light the energy of rotational states is heavily quantized:

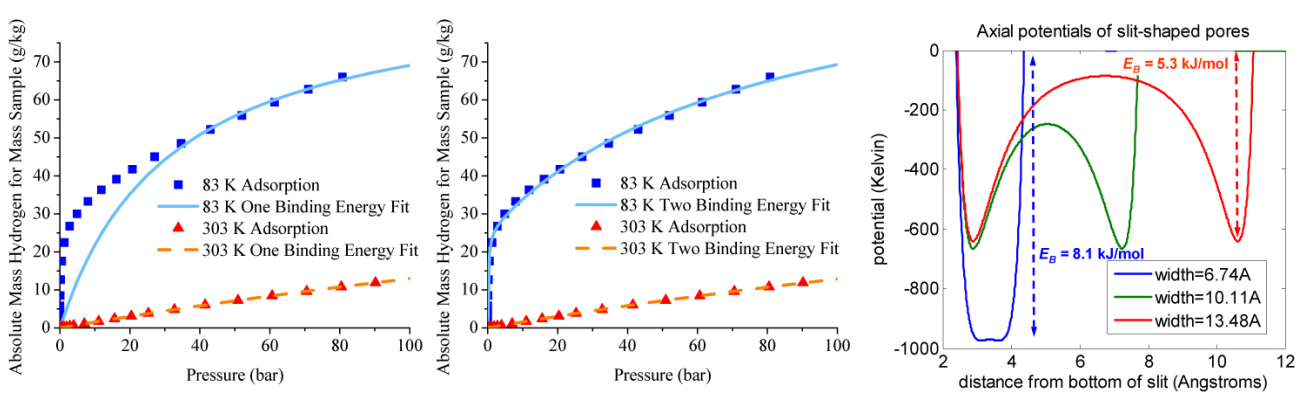

FIGURE 2. Absolute hydrogen adsorption for sample Batch 5.1. The surface area was 3,100 m^2/g, with a nanopore volume of 0.76 cm^3/g. Points are experimental. Left: single-BE fit, center: two-binding energy fit (75% of 4.8 kJ/mol, 25 % of 9.0 kJ/mol). Right: potentials of adsorption for various pore widths computed using Lennard-Jones potentials.

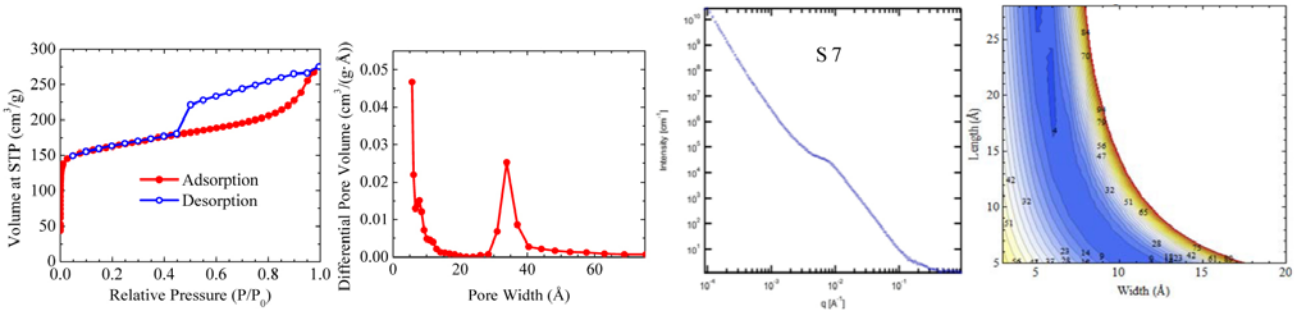

FIGURE 3. Left: N_2 adsorption isotherm for the Saran-based carbon S7 (boron-free). BET surface area is 625 m^2/g with a total pore volume of 0.43 cm^3/g. Center left: pore size distribution from DFT analysis of the adsorption isotherm. Center right: SAXS spectrum for Sample S7. Right: SAXS analysis of S7 gives an average pore dimension of 6 Å × 6Å × 17-24 Å (broad minimum in χ^2)and surface area of ~577 m^2/g, in goodagreement with the BET area.

$$E_J = J(J+1)\frac{\hbar^2}{2\mu r^2},$$

with $(E_1 - E_0)/k_B = 175$ K. Intuitively, it would appear that at low temperatures (e.g., 77 K) most H_2 molecules would remain in the $J = 0$ (spherical) state; however, the 9-fold degeneracy (nuclear spin + orbital) of the $J = 1$ state makes it relevant even at cryogenic temperatures. Intuitively, one would also expect quantum effects to be negligible at room temperature, but even at 300 K over 80% of the molecules are in the $J = 0,1$ states (Figure 4).

We considered the interaction of H_2 in each of these states with the carbon adsorbent and with other H_2 molecules. The interaction potentials become matrices with indices corresponding to the different rotational states. Figure 5 shows samples of the potentials used for our calculations. The calculations improve the quality of the computer simulations (not shown here), and the solution of Schrödinger's equation for H_2 molecules in slit-shaped pores results in energy shifts for different rotational states, which can be probed via inelastic neutron scattering. Figure 5, right, graphs the center of the scattered intensity vs. pore width. For sub-nm sized pores this gives an attractive new characterization tool, which is most sensitive where other techniques (e.g., N_2 adsorption) loose their sensitivity. We are pursuing experimental tests of these predictions.

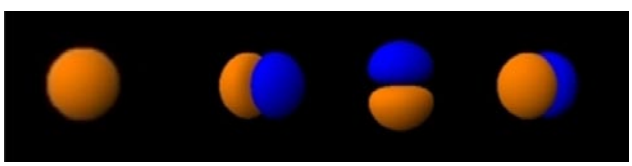

FIGURE 4. Quantum rotational states of hydrogen molecules (amplitude of probability for the states s, p_y, p_z, and p_x.

Effects of Boron Doping

Graphite does not bind hydrogen strongly (BE ~5 kJ/mol). "Engineered" nanopores may raise the BE by a factor of 2: in very narrow pores, each H_2 sees the potential of both graphene layers. Computations performed by other groups predict that boron doping of carbon raises the BE of H_2 significantly, from ~5 kJ/mol to 15-38 kJ/mol, by charge transfer from the occupied σ

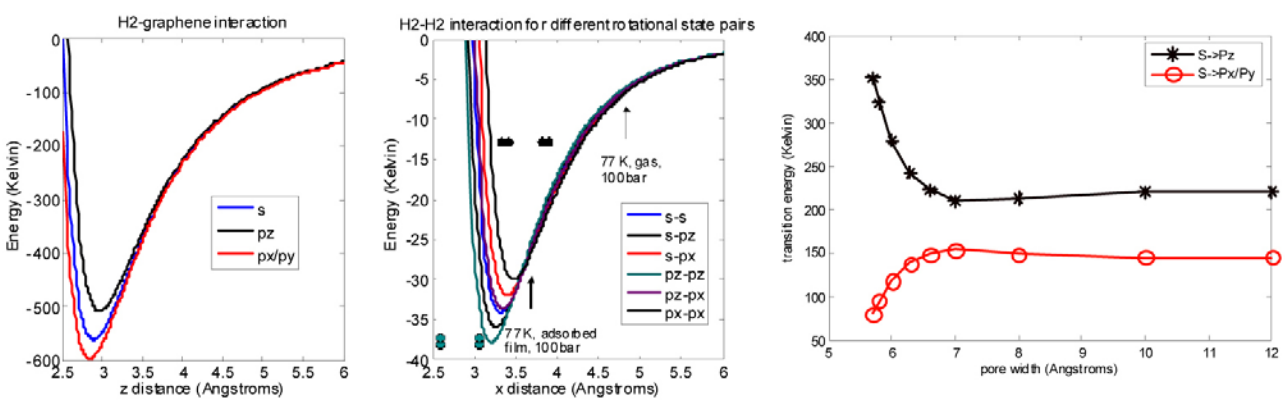

FIGURE 5. Hydrogen-graphene (left) and hydrogen-hydrogen (center) interactions for various rotational states. Right: $s \rightarrow p$ transition energies for H_2 molecules in slit-shaped nanpores vs. slit width.

orbital of H_2 to the empty pz orbital of B. In fullerenes, this generates strong-binding sites (~40 kJ/mol) (Ref. 7, Figure 3). In graphene, our calculations indicate a more modest increase, raising the BE from ~5 kJ/mol to ~8 kJ/mol, Figure 6.

Structural and energetic factors in designing a nanoporous sorbent for H_2 The combined effect of boron doping and "pore engineering" should lead to BEs close to the ideal value ~15 kJ/mol for storage and delivery of H_2 at room temperature via pressure sweeps only. Figure 7 shows adsorption isotherms for a 1.08 nm pore at 77 and 298 K for two BEs (pure carbon, 5 kJ/mol, and doped ~15 kJ/mol). A boron-doped carbon appears capable of achieving the DOE targets for H_2 storage at room temperature. Figure 7 also shows the presence of multi-layer adsorption. This may explain the large adsorption of some of the samples (Section I). Future research directions: "ensemble" calculations of many boron-carbon configurations, determination of H_2-substrate interaction for larger systems, consideration of different geometries (small graphene platelets, non-substitutional boron doping, etc).

Publications Acknowledging DOE Support

1. J. Burress, M. Kraus, M. Beckner, R. Cepel, G. Suppes, C. Wexler, and P. Pfeifer, "Hydrogen Storage in Engineered Carbon Nanospaces." *Nanotechnology* **20**, 204026 (2009).

2. L. Firlej, B. Kuchta, C. Wexler , and P. Pfeifer, "Boron substituted graphene: energy landscape for hydrogen adsorption." *Adsorption* **15** (2009), DOI 10.1007/s10450-009-9182-9.

3. B. Kuchta, L. Firlej, C. Wexler, and P. Pfeifer, "How can we reach the 2015 goals for hydrogen storage with carbon based materials?" submitted to *Langmuir* (Feb/2009).

4. P. Pfeifer, J.W. Burress, M.B. Wood, C.M. Lapilli, S.A. Barker, J.S. Pobst, R.J. Cepel, C. Wexler, P.S. Shah, M.J. Gordon, G.J. Suppes, S.P. Buckley, D.J. Radke, J. Ilavsky, A.C. Dillon, P.A. Parilla, M. Benham, and M.W. Roth, "High-Surface-Area Biocarbons for Reversible

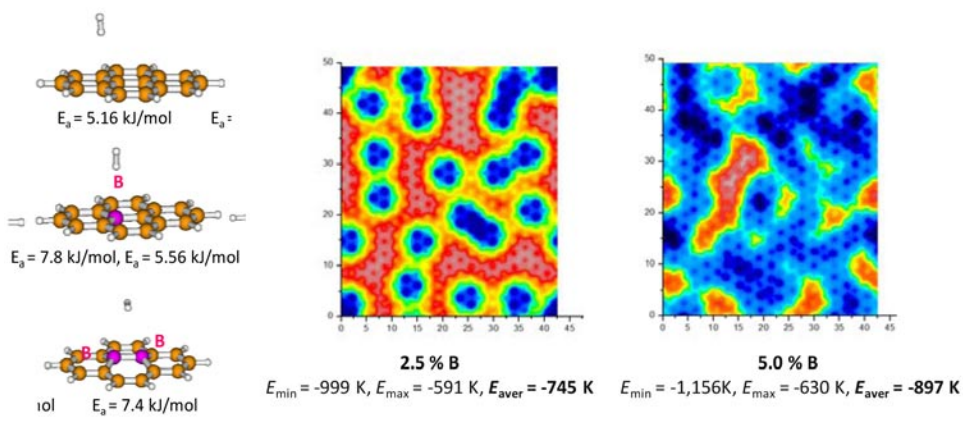

FIGURE 6. Left: H_2 binding energy in boron-doped carbon (calculated at MP2 level). Center & right: 2.5, 5.0% of carbons were substituted randomly by boron. This raises the *average* BE by ~30-50% over pure graphite.

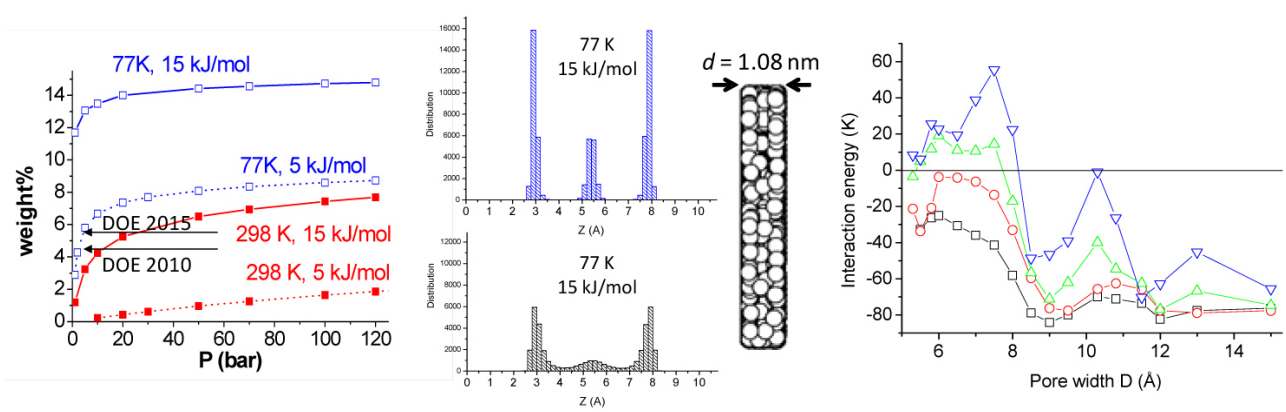

FIGURE 7. Left: Hydrogen adsorption isotherms for pure carbon (binding energy ~5 kJ/mol) and boron-doped carbon (~15 kJ/mol). Center: density profile shows formation of a third layer of H_2 due to H_2-H_2 interactions with the high-density first layers. Right: H_2-H_2 interaction energy vs. pore width for multi-layer formation.

On-Board Storage of Natural Gas and Hydrogen." In: *Life Cycle Analysis for New Energy Conversion and Storage Systems*, eds. V.M Fthenakis, A.C. Dillon, and N. Savage, *Mater. Res. Soc. Symp. Proc.* **1041**, 1041-R02-02 (2008). http://www.mrs.org/s_mrs/sec_subscribe.asp?CID=11339&DID=202443. Invited paper.

5. M.J. Connolly, M.W. Roth, P.A. Gray, and C. Wexler; "Explicit hydrogen molecular dynamics simulations of hexane deposited onto graphite at various coverages." *Langmuir* **24**, 3228-3224 (2008).

6. L. Firlej, B. Kuchta, M.W. Roth, M.J. Connolly, and C. Wexler, "Structural and phase properties of tetracosane ($C_{24}H_{50}$) monolayers adsorbed on graphite: Explicit Hydrogen Molecular Dynamics study," *Langmuir* **24**, 12392-12397 (2008).

7. L. Firlej, B. Kuchta, M.W. Roth, and C. Wexler, "Crossover mechanism of the melting transition in monolayers of alkanes adsorbed on graphite and the universality of energy scaling." submitted to *Phys. Rev. Lett.* (Feb/2009), arXiv:0902.4422.

8. C. Wexler, L. Firlej, B. Kuchta, M.W. Roth, "Melting of hexane monolayers adsorbed on graphite: the role of domains and defect formation." submitted to *Langmuir* (Mar/2009), arXiv:0903.1065.

9. O. Ciftja and C. Wexler; "Anisotropy in two-dimensional electronic quantum Hall systems at half-filled valence Landau levels." *Physica* B **403**, 1511 (2008).